ACS OMEGA

Open Access

http://pubs.acs.org/journal/acsodf

Article

Quantitative Biodistribution of OMVs Using SPECT/CT Imaging with HYNIC-Duramycin Radiolabeling

Dávid Szöllősi, Polett Hajdrik, Hedvig Tordai, Ralf Bergmann, Ildikó Horváth, Judith Mihály, Anikó Gaál, Bálint Jezsó, Kanni Das Shailaja, Tamás Felföldi, Parasuraman Padmanabhan, Balázs Zoltán Gulyás, Domokos Máthé,△ Zoltán Varga,△ and Krisztián Szigeti*,△

Cite This: *ACS Omega* 2024, 9, 42808−42813

Read Online

ACCESS | Metrics & More | Article Recommendations

ABSTRACT: *Introduction:* Bacterial outer membrane vesicles (OMVs) are emerging as important players in the host−microbiome interaction, while also proving to be a promising platform for vaccine development and targeted drug delivery. The available methods for measuring their biodistribution, however, are limited. We aimed to establish a high-efficiency radiolabeling method for the treatment of OMVs. *Methods:* ^{99m}Tc-HYNIC-duramycin was incubated with OMVs isolated from *E. coli* BL21(DE3) ΔnlpI ΔlpxM. Radiolabeling efficiency (RLE) and radiochemical purity (RCP) were measured with size-exclusion high-performance liquid chromatography. The biodistribution was quantitatively measured in mice using SPECT/CT imaging. *Results:* RLE was 81.84 ± 2.03% for undiluted OMV suspension and 56.17 ± 2.29% for 100× dilution. Postlabeling purification with a spin-desalting column results in 100% radioactivity in the OMV fraction according to HPLC, indicating 100% RCP of the final product. The biodistribution was found to be in line with previous data reported in the literature using other OMV tracking attempts. *Conclusions:* Our findings illustrate that using HYNIC-duramycin for labeling of the OMVs enhances efficiency and is easily implementable for in vivo imaging studies, significantly improving upon earlier methods.

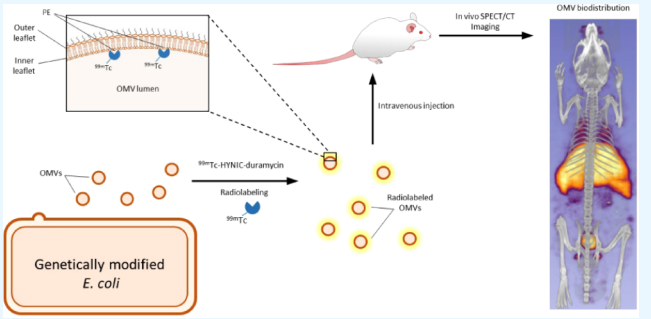

1. INTRODUCTION

Bacterial OMVs are nanoscale EVs released by Gram-negative bacteria into the environment. Their composition—protein and lipid—is similar to the bacterial outer membrane.[1,2] The role of OMVs in bacterial life and host−microbiome interactions is multifaceted, being involved in bacterial competition, gene transfer, nutrient transport, antibiotic resistance, and stress response mechanisms.[2−4] OMVs are also emerging as a versatile vaccine platform.[5,6] Genetically modified OMVs also represent a promising platform for targeted drug delivery applications due to their optimal size and shape for enhanced permeability[5] and the presence of targeting surface molecules.[6]

Our knowledge regarding their biodistribution is limited.[7−12] However, quantifying their biodistribution currently poses a challenge to researchers, as the most widely used methods are based on fluorescent labeling and measuring with either whole-body fluorescence imaging devices or microscopy.

Nuclear medicine imaging is a promising tool that may offer a solution to these challenges. Advances in imaging methods allow the in vivo quantification of radiolabeled compounds at multiple time points in the same animal coupled with high-resolution structural imaging (e.g., CT and MRI). The key to these methods is to use a reliable and high-quality radiolabeling procedure.

Radiolabeling methods for OMVs have been reported earlier.[13−16] The approach of Pastor et al.[13] is based on the classic stannous-chloride reduction of technetium with a reported >95−97% radiolabeling yield. Siddiqui et al.[14] describe a method for the radiolabeling of bacteria and OMVs for PET imaging. They demonstrated that ^{64}Cu-labeled YbT can be incorporated into FyuA-expressing bacteria and their OMVs selectively. Zhe Li et al.[15] report a deferoxamine-based ^{89}Zr-labeling method of avian pathogenic *E. coli* OMVs. Our group has previously reported an OMV radiolabeling method based on the surface display of SpyCatcher, a widely used protein ligation system.[16]

There are many more possible approaches to EV radiolabeling. A favorable approach would be one that can be used

Received: May 15, 2024
Revised: September 2, 2024
Accepted: October 4, 2024
Published: October 11, 2024

for a wide variety of bacterial strains. Such a method should target a common OMV component. Due to their biogenesis, the inner leaflet of the OMV membrane is rich in phosphatidylethanolamine (PE), which is also present in the outer leaflet in smaller quantities. Duramycin is a naturally occurring lantibiotic that binds to PE in the envelope of Gram-positive and Gram-negative bacteria.[17,18] Technetium-labeled duramycin has also been developed, and kit formulations of HYNIC-conjugated duramycin for radiolabeling are commercially available[19−25] (Figure 1). We have previously carried out

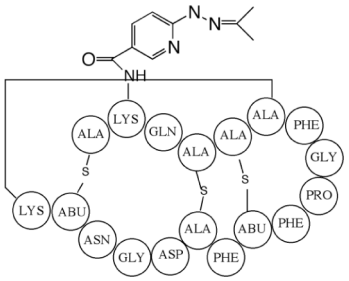

Figure 1. Structure of HYNIC-duramycin. ABU: α-aminobutyric acid.

successful duramycin-based labeling of eukaryotic EVs. However, based on our experience, most labeling approaches that generally work for eukaryotic EVs translate very poorly for OMVs due to the differences in structure.

Our aim in this study was to develop a radiolabeling method based on duramycin that enables the measurement of the OMV biodistribution using SPECT.

2. RESULTS AND DISCUSSION

2.1. Radiolabeling and Serum Stability. Our experiments were carried out on our previously developed double mutant *E. coli* BL21(DE3) ΔlpxM ΔnlpI strain which makes OMV production more efficient and has an altered LPS phenotype with reduced proinflammatory effects. The OMVs of this strain have previously been characterized by our group.[16] A TEM photomicrograph of the vesicles is presented in Figure 2.

The protein content of the OMV suspensions was measured before radiolabeling using a modified Lowry assay, which resulted in 3.24 ± 0.24 mg/mL (mean ± SD). Although these numbers indicate a high concentration, it is important to keep in mind that some remaining peptide contaminants from the culture medium and the choice of protein assay can highly influence perceived OMV protein content.[16] Before OMV radiolabeling, HYNIC-duramycin was radiolabeled with freshly eluted ^{99m}Tc following the manufacturer's instructions resulting in >95% RCP. Next, the radiolabeled HYNIC-duramycin solution was mixed with a dilution series of an OMV isolate and incubated at 37 °C to let duramycin bind to the PE present in the OMVs. The suspensions were applied to preparative spin-desalting columns to separate the vesicles from unreacted duramycin and other contaminants. To estimate RLE, the ratio of eluate activity to the sum of eluate and column activities was calculated. Our results suggest a sublinear dependence of RLE on the concentration of the OMV in the investigated concentration range (Figure 3A): 56.17 ± 2.29% efficiency at 1% OMV concentration and 81.84 ± 2.03% efficiency at 100% OMV concentration. We also compared the radiochemical purity (RCP) before and after desalting using SEC-HPLC (Figure 3B). Prior to desalting, a

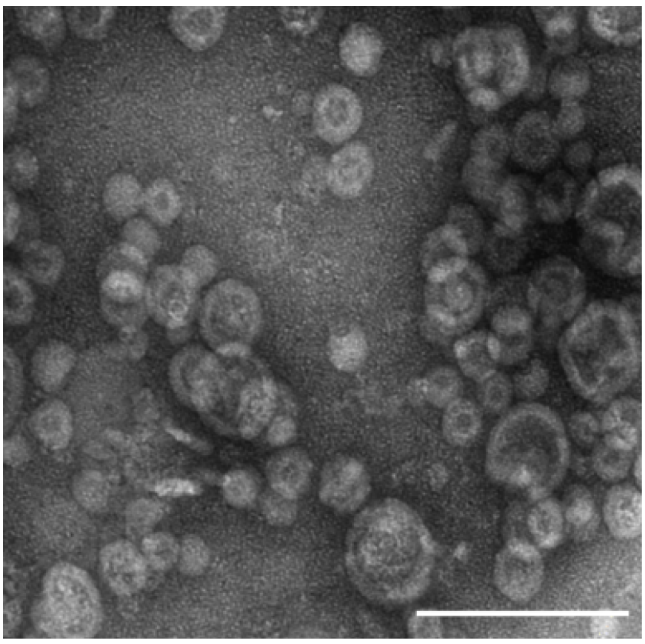

Figure 2. OMV characterization results: TEM photomicrograph. The scale bar represents 100 nm.

second peak was observable, which was entirely removed after desalting, resulting in 100% RCP (Figure 3B). We did not observe any increase in the RCP of the 1% sample measured 10 min apart (58.82% initially and 54.85% for the same sample measured 10 min later), suggesting that the radiolabeling reaction has reached a plateau. All further experiments were done by radiolabeling the OMV suspension without dilution (100%). To mimic serum conditions, we have incubated freshly radiolabeled vesicles purified using a Zeba spin-desalting column in fetal bovine serum (FBS) in a ratio of 2:8 (OMV:FBS) at 37 °C, shaking. We sampled the mixture for SEC-HPLC analysis every 20 min up to 125 min after the start of incubation. This experiment was done in triplicates. The radiochromatograms showed no considerable change during this time period, still having no second peak, indicating that radiolabeling has 100% stability during the timeline of the experiment (Figure 3C).

2.2. In Vivo Imaging. Using the radiolabeled OMVs, we carried out SPECT/CT measurements to assess the biodistribution of their biomaterials (Figure 4). Preclinical SPECT has multiple advantages over optical imaging methods often used for EV biodistribution studies. The small animal SPECT studies can be readily scaled up to human medicine. The use of CT or MRI-based attenuation and scatter correction coupled with novel reconstruction methods make SPECT a quantitative imaging modality.

The radiolabeled OMV isolates were intravenously administered to two BALB/c mice via the lateral tail vein. SPECT/CT images were acquired 90 min p.i. to determine the in vivo stability and biodistribution of the OMVs (Figure 4a,b). Mice were closely monitored for 4 h following the injection of radiolabeled OMVs. We did not observe any signs of systemic inflammation in this period. Organ activities and activity concentrations, both normalized to an injected dose (ID), are presented in Figure 4. The liver uptake was the highest, accounting for 62.75% of the ID, reaching 0.47%ID/ml. The spleen and bladder activities were also high, with 3.85% and

https://doi.org/10.1021/acsomega.4c04632
ACS Omega 2024, 9, 42808−42813

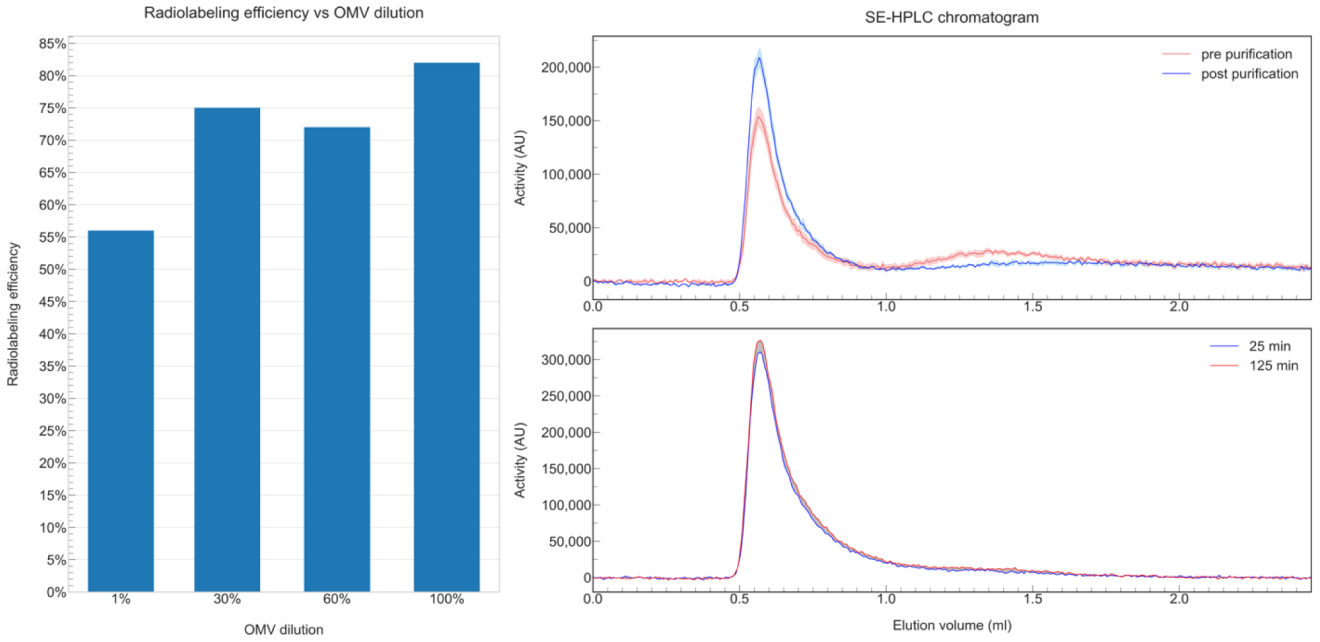

Figure 3. OMV radiolabeling results. (A) The radiolabeling efficiency shows a strong dependence on the OMV dilution. (B) Radio-SEC-HPLC chromatogram of the radiolabeled undiluted OMV suspension before (red) and after spin-desalting (solid line = mean; light colored area = mean ± SEM). The lack of the second peak after purification indicates 100% radiochemical purity of the product. Chromatograms were scaled to correct slight differences in dilution. (C) Radio-SEC-HPLC chromatograms of radiolabeled OMVs taken after 25 and 125 min of incubation in FBS. Solid lines represent the mean values of 3 chromatograms. The difference between the two curves is shaded gray.

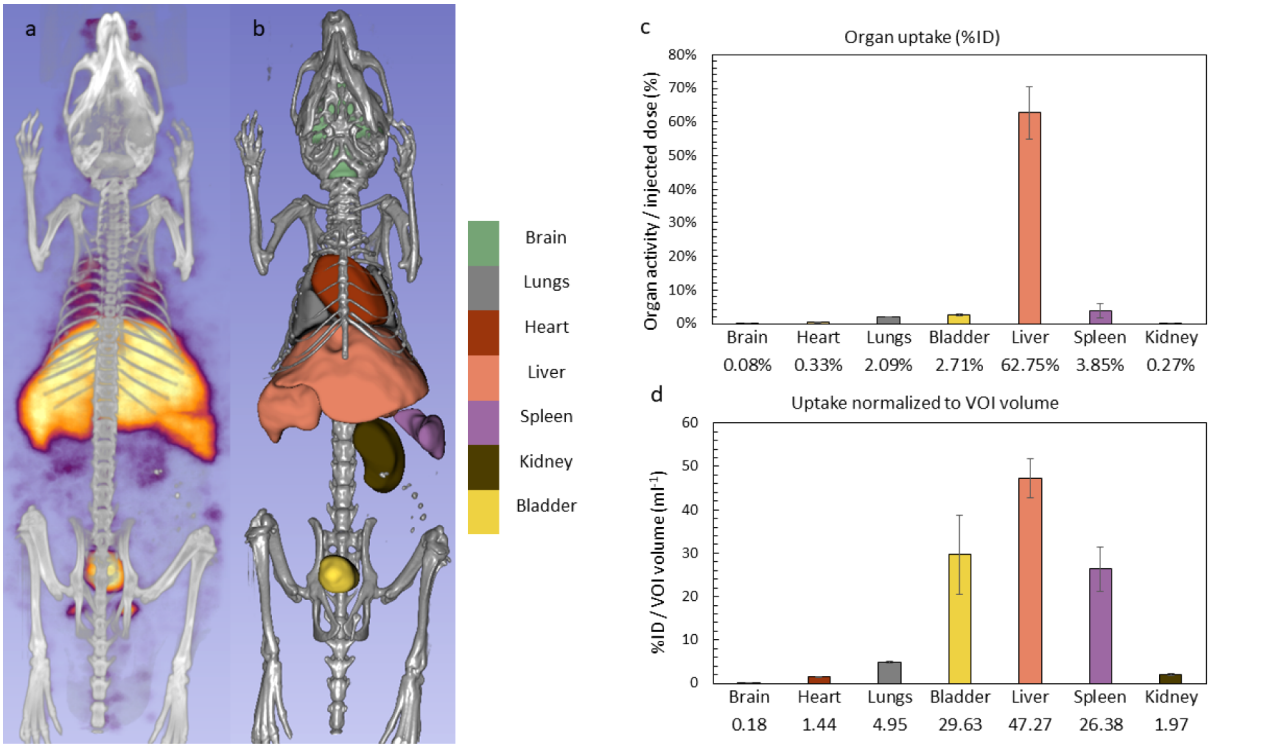

Figure 4. In vivo imaging results. (a) A maximum intensity projection (MIP) of a SPECT/CT image showing the distribution of radiolabeled OMVs 90 min postinjection. (b) A surface-rendered image depicting the position of VOI's used for the quantification of OMV biodistribution. Organ uptake data are represented as the percentage of the injected dose (c) and the percentage of the injected dose normalized to VOI volume (d). Bars represent the mean, while error bars represent the min and max of the two animals.

2.71% of the ID, respectively, and with a mean activity concentration of 0.26 and 0.30%ID/ml, respectively. All other organs measured (brain, heart, lungs, and kidney) had very low uptake (Figure 4 c,d). The pattern of biodistribution—enrichment in the liver and spleen—is similar to previously reported OMV biodistribution data.[9,10] Differences in delivery methods, imaging time, and imaging modalities mean that a fair comparison cannot be made unequivocally. The most

https://doi.org/10.1021/acsomega.4c04632
ACS Omega 2024, 9, 42808−42813

prominent feature of HYNIC-duramycin's distribution pattern in rodents is the kidney uptake which remains highly elevated for at least 8 h postinjection according to previously published data.[19,20,26−28] The very low uptake (1.19%ID/ml 2 h p.i.) measured during our experiments suggests that [^{99m}Tc]-HYNIC-duramycin did not dissociate from the OMVs in vivo. We also did not observe any thyroid or stomach uptake that would indicate free pertechnetate.

A possible limitation to our approach could be the reliability on duramycin's ability to bind to the OMVs. At first, it might seem logical to assume that this labeling would only work on OMVs isolated from duramycin-sensitive bacterial strains; however, a recent study revealed that duramycin can even bind to the membrane of a resistant strain and sensitivity does not only depend on PE content.[17] Also, to determine the amount of OMVs in a given volume based on these results, more data would be needed regarding the size dependence of the OMV PE/lipid ratio and duramycin binding affinity.

In conclusion, we have demonstrated that ^{99m}Tc-labeled HYNIC-duramycin can be used to radiolabel OMVs for in vivo SPECT imaging. Due to the availability of commercial kits, radiolabeling is easy to carry out with a high RLE, and postlabeling purification using a spin-desalting column results in 100% radiochemical purity. We believe that our method could also be adapted to PET imaging by changing the HYNIC group to a suitable chelator (e.g., NODA-GA).

3. MATERIALS AND METHODS

3.1. Culture Conditions. Lysogeny broth was used for *E. coli* BL21(DE3) ΔnlpI ΔlpxM cultures.[16] An amount of 25 g of lysogeny broth (Miller) powder (Sigma-Aldrich, USA) was dissolved in 1 L of Milli-Q water, and the pH was adjusted to 7.0 with NaOH before autoclaving.

3.2. Outer Membrane Vesicle Isolation. For OMV isolation, a combination of ultrafiltration, tangential flow filtration, and ultracentrifugation was used.[16] Briefly, 2 × 250 mL starter cultures were incubated at 37 °C and 180 rpm shaking for 16 h. After OD600 measurement, the pooled culture was centrifuged at 5000 g for 15 min at 4 °C to pellet the bacteria. After the supernatant was filtered using a vacuum filter with 0.45 μm pore size, a stirred-cell ultrafiltration device equipped with a 100 kDa MWCO ultrafiltration disc was used to concentrate it to 60 mL. The volume of the concentrate was further reduced using a TFF-easy device (Hansa Biomed, Estonia) to ∼5 mL. After washing the concentrate with 60 mL of PBS with TFF, it was ultracentrifuged for 2 h at 150000 g, 4 °C, using an XL-80 ultracentrifuge with a Type 50.2 Ti rotor (Beckman-Coulter, USA). The pellet was resuspended in 500 μL of PBS and filtered using a Costar Spin-X 0.45 μm centrifuge filter (Corning, USA). OMV isolates were stored at 4 °C for up to 4 weeks.

Protein content was determined with a Lowry kit (Thermo Fisher Scientific, USA) using a 96-well microplate working in triplicates. Absorbance was measured with a BioTek (USA) Synergy 2 plate reader.

The quality of OMV isolates was checked using SDS gel electrophoresis (15%, SDS-PAGE) and transmission electron microscopy (TEM) as described elsewhere.[16]

3.3. Radiolabeling and Serum Stability. HYNIC-duramycin kits were purchased from Molecular Targeting Technologies (USA). Briefly, 0.5 mL of freshly eluted ^{99m}Tc-pertechnetate (4.047 GBq eluted from an Ultra-Technekow FM 2.15−43.00 GBq technetium generator (Curium, Netherlands) solution was applied to the glass vial of the kit. The vial was incubated at 80 °C for 20 min to complete labeling, resulting in a specific activity of 262 MBq/μg as confirmed with reversed-phase HPLC. A dilution series was made from the OMV suspension in PBS (100%, 60%, 30%, and 1%). A volume of 50 μL of radiolabeled [^{99m}Tc]HYNIC-duramycin was mixed with 50 μL of each OMV sample and incubated for 30 min at 37 °C, 200 rpm shaking, in a neoMix cool thermomixer (Neolab, Germany). Excess duramycin was removed using 0.5 mL 40 kDa MWCO Zeba spin-desalting columns (Thermo Scientific, USA) equilibrated with PBS according to the manufacturer's instructions. The radioactivity of the eluates and columns was measured using an ISOMED 2010 dose calibrator (Nuvia, France). Radiolabeling efficiency (RLE) was calculated as the ratio of eluate activity and total activity of column + eluate.

To test the serum stability of the radiolabeled OMVs, 3 × 20 μL of the radiolabeled 100% OMV sample was mixed with 3 × 80 μL of Gibco fetal bovine serum (Thermo Fisher, USA) and incubated at 37 °C, 200 rpm shaking, in a neoMix cool thermomixer (Neolab, Germany). Starting at 25 min post-incubation, 10 μL samples were taken every 20 min and analyzed with size-exclusion high-performance chromatography.

3.4. High-Performance Liquid Chromatography. Radiolabeled samples were analyzed using either RP-HPLC or SE-HPLC. A Jasco HPLC system was equipped with a PU-2089 pump, a UV-2089 UV detector, and a gamma-RAM Model 4 radio-HPLC detector (LabLogic, USA).

A Chromolith FastGradient RP-18e 50-2 mm column (Supelco, USA) was used to measure the radiochemical purity of ^{99m}Tc-HYNIC-duramycin. Milli-Q water with 0.1% trifluoroacetic acid (solvent A) and 100% acetonitrile (solvent B) were used as mobile phases. A sample volume of 1 μL was used, and the gradient elution protocol was as follows: 0−5 min: 100% solvent A, 5−10 min: 0−80% solvent B, 13−15 min: 80%−0% solvent B, and 15−18 min: 100% solvent A. A flow rate of 0.320 mL/min was used.

A Tricorn-5/50 column with a bed volume of ∼1 mL (Cytiva, Germany) packed with Sepharose CL-4B (Cytiva, Germany) was used for each OMV measurement. PBS (pH 7.4) was used as the mobile phase. The flow rate was set to 0.5 mL/min for the total elution time of 5 min per chromatogram. Samples were diluted in PBS to ∼50 kBq/μL, and a sample volume of 10 μL was injected. Chromatograms were background- and decay-corrected. RLE was determined as the ratio of the areas under the first peak (corresponding to OMVs eluted with the void volume) and the entire chromatogram (also containing small particles eluted with total volume).

3.5. In Vivo Imaging. Two healthy 6-week-old male BALB/c mice (body weight = 18.2 and 19.3 g) were used for biodistribution studies. All procedures were conducted in accordance with the ARRIVE guidelines and the guidelines set by the Animal Care and Use Committee of the IEM and Semmelweis University (PE/EA/929-5/2021). A volume of 120 μL of radiolabeled OMV suspension with an activity of 54.9 ± 15.55 MBq (mean ± SD) was administered intravenously into the lateral tail vein. Mice were anesthetized with isoflurane (1.5%) for the whole duration of imaging. SPECT/CT (nanoScan SPECT/CT (Mediso, Hungary)) equipped with multipinhole mouse collimators. Helical CT scan settings: 50 kVp and 980 μ, 300 ms exp time, 1:4 binning,

https://doi.org/10.1021/acsomega.4c04632
ACS Omega 2024, 9, 42808−42813

pitch 1, zoom factor 1.2, and 687 projections (360 projections/rotation). Static SPECT scan settings: 90 min p.i. using a 30 s frame time, zoom factor 1.43, 120 frames in 2 rotations, and 4 detectors. CT images were reconstructed with an iterative algorithm using 30 iterations and 0.13 mm isovoxel. SPECT images were iteratively reconstructed with a medium filter: 64 iterations and 0.12 mm isovoxel. VOIs were manually delineated around the selected organs (brain, lungs, heart, liver, spleen, kidney, and bladder). VOI uptake data are reported in % organ activity/injected dose and % organ activity/(injected dose × VOI volume).

3.6. Data Analysis. All numerical data were organized with Microsoft Excel (Microsoft, USA). Analysis and illustration were done in python 3 using pandas,[29] numpy,[30] and matplotlib.[31]

AUTHOR INFORMATION

Corresponding Author

Krisztián Szigeti − *Department of Biophysics and Radiation Biology, Semmelweis University, Budapest 1094, Hungary;* orcid.org/0000-0002-0828-9828; Phone: +36-20-663-2113; Email: krisztian.szigeti@gmail.com

Authors

Dávid Szöllősi − *Department of Biophysics and Radiation Biology, Semmelweis University, Budapest 1094, Hungary;* orcid.org/0000-0002-3363-3862

Polett Hajdrik − *Department of Biophysics and Radiation Biology, Semmelweis University, Budapest 1094, Hungary*

Hedvig Tordai − *Department of Biophysics and Radiation Biology, Semmelweis University, Budapest 1094, Hungary*

Ralf Bergmann − *Department of Biophysics and Radiation Biology, Semmelweis University, Budapest 1094, Hungary*

Ildikó Horváth − *Department of Biophysics and Radiation Biology, Semmelweis University, Budapest 1094, Hungary*

Judith Mihály − *Biological Nanochemistry Research Group, HUN-REN Research Centre for Natural Sciences, Institute of Materials and Environmental Chemistry, Budapest 1117, Hungary*

Anikó Gaál − *Biological Nanochemistry Research Group, HUN-REN Research Centre for Natural Sciences, Institute of Materials and Environmental Chemistry, Budapest 1117, Hungary*

Bálint Jezsó − *Molecular Cell Biology Research Group, Institute of Enzymology, Research Center for Natural Sciences, Budapest 1117, Hungary*

Kanni Das Shailaja − *Department of Biophysics and Radiation Biology, Semmelweis University, Budapest 1094, Hungary*

Tamás Felföldi − *Department of Microbiology, ELTE Eötvös Loránd University, Budapest 1117, Hungary; Institute for Aquatic Ecology, HUN-REN Centre for Ecological Research, Budapest 1113, Hungary;* orcid.org/0000-0003-2009-2478

Parasuraman Padmanabhan − *Lee Kong Chian School of Medicine, Nanyang Technological University, Singapore 636921, Singapore; Cognitive Neuroimaging Centre, Singapore 636921, Singapore;* orcid.org/0000-0003-4112-4600

Balázs Zoltán Gulyás − *Lee Kong Chian School of Medicine, Nanyang Technological University, Singapore 636921, Singapore; Cognitive Neuroimaging Centre, Singapore 636921, Singapore*

Domokos Máthé − *Department of Biophysics and Radiation Biology, Semmelweis University, Budapest 1094, Hungary; CROmed Translational Research Centers, Budapest 1094, Hungary; In Vivo Imaging Advanced Core Facility, Hungarian Center of Excellence for Molecular Medicine (HCEMM), Budapest 1094, Hungary*

Zoltán Varga − *Department of Biophysics and Radiation Biology, Semmelweis University, Budapest 1094, Hungary; Biological Nanochemistry Research Group, HUN-REN Research Centre for Natural Sciences, Institute of Materials and Environmental Chemistry, Budapest 1117, Hungary; Department of Physical Chemistry and Materials Science, Faculty of Chemical Technology and Biotechnology, Budapest University of Technology and Economics, H-1111 Budapest, Hungary*

Complete contact information is available at: https://pubs.acs.org/10.1021/acsomega.4c04632

Author Contributions

△D. M., Z.V., and K.S. contributed equally.

Notes

The authors declare no competing financial interest.

ACKNOWLEDGMENTS

The research received funding from the Hungarian National Research, Development and Innovation Office (OTKA grant K 131594), the János Bolyai Research Felowship of the Hungarian Academy of Sciences (ZV, TF), and from the ÚNKP-20-5 and ÚNKP-21-5 Bolyai+ New National Excellence Programs of the Ministry for Innovation and Technology from the source of the National Research, Development and Innovation Fund (ZV), from the Higher Education Institutional Excellence Program of the Ministry of Human Resources in Hungary, within the framework of the Therapeutic Development thematic program of Semmelweis University, and the European Union's Horizon 2020 research and innovation program under grant agreement No 739593. HCEMM was supported by the EU Program: H2020-EU.4.a and SmartAge GA Nr. 859890. This work was also partly funded by grants from the Hungarian National Research, Development and Innovation Office (Thematic Excellence Program, TKP-BIOImaging, financed under the 2020-4.1.1-TKP2020 funding scheme), 2020-1-1-2-PIACI-KFI_2020-00021, TKP2021-EGA-31, VEKOP-2.3.3-15−2016- 00005, and 2022-1.1.1-KK-2022-00005. The authors would like to thank Prof. Miklós Geiszt for help with imaging studies.

4.ABBREVIATIONS

CT, computed tomography; EV, extracellular vesicle; FBS, fetal bovine serum; HPLC, high-performance liquid chromatography; HYNIC, hydrazinonicotinic acid; ID, injected dose; LPS, lipopolysaccharide; MRI, magnetic resonance imaging; MWCO, molecular weight cutoff; OMV, outer membrane vesicle; PE, phosphatidylethanolamine; PET, positron emission tomography; RCP, radiochemical purity; RLE, radiolabeling efficiency; RP-HPLC, reversed-phase HPLC; RPM, revolutions per minute; SDS-PAGE, sodium dodecyl sulfate polyacrylamide gel electrophoresis; SEC-HPLC, size exclusion HPLC; SPECT, single-photon emission computed tomography; TFF, tangential flow filtration; VOI, volume of interest

https://doi.org/10.1021/acsomega.4c04632
ACS Omega 2024, 9, 42808−42813

REFERENCES

(1) Avila-Calderon, E. D.; Ruiz-Palma, M. D. S.; Aguilera-Arreola, M. G.; Velazquez-Guadarrama, N.; Ruiz, E. A.; Gomez-Lunar, Z. Outer Membrane Vesicles of Gram-Negative Bacteria: An Outlook on Biogenesis. *Front. Microbiol.* **2021**, *12*, 557902.

(2) Bonnington, K. E.; Kuehn, M. J. Protein selection and export via outer membrane vesicles. *Biochim. Biophys. Acta* **2014**, *1843*, 1612−1619.

(3) Schwechheimer, C.; Kuehn, M. J. Outer-membrane vesicles from Gram-negative bacteria: biogenesis and functions. *Nat. Rev. Microbiol.* **2015**, *13*, 605−619.

(4) Caruana, J. C.; Walper, S. A. Bacterial Membrane Vesicles as Mediators of Microbe − Microbe and Microbe − Host Community Interactions. *Front. Microbiol.* **2020**, *11*, 432.

(5) Gerritzen, M. J. H.; Martens, D. E.; Wijffels, R. H.; van der Pol, L.; Stork, M. Bioengineering bacterial outer membrane vesicles as vaccine platform. *Biotechnol. Adv.* **2017**, *35*, 565−574.

(6) Chang-Monteagudo, A.; Ochoa-Azze, R.; Climent-Ruiz, Y.; Macias-Abraham, C.; Rodriguez-Noda, L.; Valenzuela-Silva, C. A single dose of SARS-CoV-2 FINLAY-FR-1A vaccine enhances neutralization response in COVID-19 convalescents, with a very good safety profile: An open-label phase 1 clinical trial. *Lancet Reg. Health Am.* **2021**, *4*, 100079.

(7) Jang, S. C.; Kim, S. R.; Yoon, Y. J.; Park, K. S.; Kim, J. H.; Lee, J. In vivo kinetic biodistribution of nano-sized outer membrane vesicles derived from bacteria. *Small* **2015**, *11*, 456−461.

(8) Kim, O. Y.; Park, H. T.; Dinh, N. T. H.; Choi, S. J.; Lee, J.; Kim, J. H.; Lee, S.-W.; Gho, Y. S. Bacterial outer membrane vesicles suppress tumor by interferon-γ-mediated antitumor response. *Nat. Commun.* **2017**, *8*, 626.

(9) Jones, E. J.; Booth, C.; Fonseca, S.; Parker, A.; Cross, K.; Miquel-Clopes, A.; Hautefort, I.; Mayer, U.; Wileman, T.; Stentz, R.; et al. The Uptake, Trafficking, and Biodistribution of Bacteroides thetaiotaomicron Generated Outer Membrane Vesicles. *Front. Microbiol.* **2020**, *11*, 57.

(10) Huang, Y.; Beringhs, A. O. R.; Chen, Q.; Song, D.; Chen, W.; Lu, X. Genetically Engineered Bacterial Outer Membrane Vesicles with Expressed Nanoluciferase Reporter for in Vivo Bioluminescence Kinetic Modeling through Noninvasive Imaging. *ACS Appl. Bio Mater.* **2019**, *2*, 5608−5615.

(11) Gujrati, V.; Kim, S.; Kim, S. H.; Min, J. J.; Choy, H. E.; Kim, S. C. Bioengineered bacterial outer membrane vesicles as cell-specific drug-delivery vehicles for cancer therapy. *ACS Nano* **2014**, *8*, 1525−1537.

(12) Kuerban, K.; Gao, X.; Zhang, H.; Liu, J.; Dong, M.; Wu, L. Doxorubicin-loaded bacterial outer-membrane vesicles exert enhanced anti-tumor efficacy in non-small-cell lung cancer. *Acta Pharm. Sin. B* **2020**, *10*, 1534−1548.

(13) Pastor, Y.; Larraneta, E.; Erhard, Á.; Quincooces, G.; Penuelas, I.; Irache, J. M.; Donnelly, R.; Gamazo, C. Dissolving Microneedles for Intradermal Vaccination against Shigellosis. *Vaccines* **2019**, *7*, 159.

(14) Siddiqui, N. A.; Houson, H. A.; Thomas, S. C.; Blanco, J. R.; O'Donnell, R. E.; Hassett, D. J. Radiolabelled Bacterial Metallophores as Targeted PET Imaging Contrast Agents for Accurate Identification of Bacteria and Outer Membrane Vesicles in vivo. *bioRxiv* **2020**.

(15) Li, Z.; Niu, L.; Wang, L.; Mei, T.; Shang, W.; Cheng, X. Biodistribution of (89)Zr-DFO-labeled avian pathogenic *Escherichia coli* outer membrane vesicles by PET imaging in chickens. *Poult. Sci.* **2023**, *102*, 102364.

(16) Szöllősi, D.; Hajdrik, P.; Tordai, H.; Horváth, I.; Veres, D.; Gillich, B.; Shailaja, K. D.; Smeller, L.; Bergmann, R.; Bachmann, M.; et al. Molecular imaging of bacterial outer membrane vesicles based on bacterial surface display. *Sci. Rep.* **2023**, *13*, 18752.

(17) Hasim, S.; Allison, D. P.; Mendez, B.; Farmer, A. T.; Pelletier, D. A.; Retterer, S. T.; Campagna, S. R.; Reynolds, T. B.; Doktycz, M. J. Elucidating Duramycin's Bacterial Selectivity and Mode of Action on the Bacterial Cell Envelope. *Front. Microbiol.* **2018**, *9*, 219.

(18) Epand, R. M.; Walker, C.; Epand, R. F.; Magarvey, N. A. Molecular mechanisms of membrane targeting antibiotics. *Biochim. Biophys. Acta* **2016**, *1858*, 980−987.

(19) Zhao, M.; Li, Z. A single-step kit formulation for the (99m)Tc-labeling of HYNIC-Duramycin. *Nucl. Med. Biol.* **2012**, *39*, 1006−1011.

(20) Liu, Z.; Larsen, B. T.; Lerman, L. O.; Gray, B. D.; Barber, C.; Hedayat, A. F. Detection of atherosclerotic plaques in ApoE-deficient mice using (99m)Tc-duramycin. *Nucl. Med. Biol.* **2016**, *43*, 496−505.

(21) Luo, R.; Niu, L.; Qiu, F.; Fang, W.; Fu, T.; Zhao, M.; Zhang, Y.-J.; Hua, Z.-C.; Li, X.-F.; Wang, F. Monitoring Apoptosis of Breast Cancer Xenograft After Paclitaxel Treatment With 99mTc-Labeled Duramycin SPECT/CT. *Mol. Imaging* **2016**, *15*, 1536012115624918.

(22) Clough, A. V.; Audi, S. H.; Haworth, S. T.; Roerig, D. L. Differential lung uptake of 99mTc-hexamethylpropyleneamine oxime and 99mTc-duramycin in the chronic hyperoxia rat model. *J. Nucl. Med.* **2012**, *53*, 1984−1991.

(23) Zhang, Y.; Stevenson, G. D.; Barber, C.; Furenlid, L. R.; Barrett, H. H.; Woolfenden, J. M. Imaging of rat cerebral ischemia-reperfusion injury using(99m)Tc-labeled duramycin. *Nucl. Med. Biol.* **2013**, *40*, 80−88.

(24) Wang, L.; Wang, F.; Fang, W.; Johnson, S. E.; Audi, S.; Zimmer, M. The feasibility of imaging myocardial ischemic/reperfusion injury using (99m)Tc-labeled duramycin in a porcine model. *Nucl. Med. Biol.* **2015**, *42*, 198−204.

(25) Wu, J. C.; Qin, X.; Neofytou, E. Radiolabeled Duramycin: Promising Translational Imaging of Myocardial Apoptosis. *JACC Cardiovasc. Imaging* **2018**, *11*, 1834−1836.

(26) Elvas, F.; Vangestel, C.; Rapic, S.; Verhaeghe, J.; Gray, B.; Pak, K. Characterization of [(99m)Tc]Duramycin as a SPECT Imaging Agent for Early Assessment of Tumor Apoptosis. *Mol. Imaging Biol.* **2015**, *17*, 838−847.

(27) Zhao, M.; Li, Z.; Bugenhagen, S. 99mTc-labeled duramycin as a novel phosphatidylethanolamine-binding molecular probe. *J. Nucl. Med.* **2008**, *49*, 1345−1352.

(28) Palmieri, L.; Elvas, F.; Vangestel, C.; Pak, K.; Gray, B.; Stroobants, S. [(99m)Tc]duramycin for cell death imaging: Impact of kit formulation, purification and species difference. *Nucl. Med. Biol.* **2018**, *56*, 1−9.

(29) McKinney, W. Others. Data structures for statistical computing in python. *Proceedings of the 9th Python in Science Conference*, American College of Cardiology Foundation, 2010.

(30) Harris, C. R.; Millman, K. J.; van der Walt, S. J.; Gommers, R.; Virtanen, P.; Cournapeau, D. Array programming with NumPy. *Nature* **2020**, *585*, 357−362.

(31) Hunter, J. D. Matplotlib: A 2D Graphics Environment. *Comput. Sci. Eng.* **2007**, *9*, 90−95.

https://doi.org/10.1021/acsomega.4c04632
ACS Omega 2024, 9, 42808−42813